

An Investigation into Melt Pool Effective Thermal Conductivity for Thermal Modeling of Powder-Bed Electron Beam Additive Manufacturing

Subin Shrestha, Bo Cheng and Kevin Chou

Mechanical Engineering Department
The University of Alabama
Tuscaloosa, AL 35487

Abstract

In this study, the effective thermal conductivity of a melt pool in the powder-bed electron beam additive manufacturing (EBAM) process was investigated using a numerical technique. Although a thermo-fluid model is preferred to predict the melt pool flow, computational cost is high. The alternative is to use an effective thermal conductivity that may capture the convection effect from the melt pool flow. Using finite volume method, first a thermo-fluid model was developed to simulate process temperatures in EBAM using Ti-6Al-4V powder and validated against experiment. Separately, a thermal simulation using an effective thermal conductivity for the liquid phase was conducted. The value of the effective thermal conductivity in the thermal simulation was adjusted so that the thermal responses approach those from the validated thermo-fluid simulations. The results show that the accuracy of thermal model depends on the process parameter. Maximum error of 35% was observed for beam diameter 0.55 mm.

Keywords: Effective thermal conductivity, Electron Beam Additive Manufacturing, Marangoni effect, Thermo-fluid model.

1. Introduction

Additive manufacturing (AM) is a group of technologies which can build parts directly from digital data using a variety of material adjoining methods. Powder-bed electron beam additive manufacturing (EBAM) is a metal AM technology which utilizes a high-energy moving electron beam to fuse metal powder in a predefined manner to produce a physical part in a layer-by-layer fashion under a vacuum environment. EBAM is one of a few metal AM technologies that can make metallic parts with almost 100% density, which extended this technology in variety of industries such as aeronautic and medical fields. Due to the “adding-material” feature, EBAM has many benefits in part fabrications such as geometric design freedom, tooling-free and complex internal features. However, there are still challenges such as severe overhang deformations and regional high stresses in build parts, partially due to the inevitable rapid heating-cooling cycle in the manufacturing process.

EBAM is a complex physical phenomenon in which heat and mass transfer occurs along with the phase change. Experimental study may not be a cost effective way to study the EBAM process as it depends on various input parameters such as beam speed, beam current etc. Therefore, numerical models are developed to minimize the need of experimental study and predict the process thermal response as well as melting flow behavior. However, accurate simulation of fluid dynamics in melt pool often incurs high computational cost. Therefore pure thermal model which ignores the molten flow is usually used to save computational effort.

Meanwhile, it is necessary to compensate for the convection heat transfer due to melt pool flow in pure thermal model. Thus, effective thermal conductivity, which enhances the rate of heat transfer in melt pool, is used to incorporate the effect of convection heat transfer.

There has been a pool of studies on numerical modeling of AM process. Relatively more studies in laser based process can be found in literatures. Korner et al. [1] developed a 2D lattice Boltzmann model to investigate melting and solidification of selective beam melting (SLM) process. They have generated the process map and the results showed that packing density of powder bed had the most significant effect on melt pool characteristics. Yuan and Gu [2] created thermo-fluid model to study the temperature evolution and melt pool in SLM process. The effects of Marangoni convection and processing parameters such as laser power and scanning speed were studied. It is observed that the Marangoni convection had a significant effect on the mass and heat transfer within melt pool and the flow effect could result in wider and shallower melt pool. Cheng and Chou [3] numerically studied the scanning island size effect on melt pool geometry evolution in a SLM process. The model considered the effective conductivity in melt pool. A comprehensive thermal analysis literature review of laser based selective melting/sintering process has been conducted by Zeng et al [4], numerical modeling methods and temperature measurements have been detailed. In the field of electron beam melting process, several numerical models have also been developed. Mahale [5] developed 3D EBAM model using finite element method and finite difference method. A point heat source was applied in the model with temperature dependent Al 7075 material properties. Zäh and Lutzmann [6] developed a 3D model incorporating volumetric heat source to carry out thermal analysis of EBAM process. Various combination of scan speed and beam power was applied to study melt pool shape characteristics. Cheng et al. [7] developed a 3D thermal model using effective thermal conductivity to study process temperature and melt pool shape. The results are comparable with the experimental data and the powder porosity is found to be most critical to the thermal characteristics. In addition, Jamshidinia et al. [8] developed and compared 3D thermal and thermo-fluid numerical models. The negative surface tension gradient induced outward flow resulted in a melt pool of higher width and lower depth.

Mizikar [9] pioneered the idea of effective thermal conductivity method. The thermal conductivity of steel was modified to incorporate the fluid flow heat transfer in liquid pool. The thermal conductivity of mushy zone and liquid steel is increased by factor A. The concept of effective thermal conductivity has then been followed by different researchers. Oksman et al. [10] have calculated the actual flow field, heat transfer and solidification using a computational fluid dynamics (CFD) model. This model was then used as a basis to formulate effective thermal conductivity of steel. Taylor et al. [11] have adjusted the liquid thermal conductivity while modeling welding phenomenon to account for the heat transfer due to convection. Similarly, De and DebRoy [12] have studied the effective thermal conductivity as an uncertain parameter whose value should be adjusted by trial and error method, so as to be in agreement with corresponding experimental results.

In this study, both 3D thermal and thermo-fluid models have been developed by incorporating a conical volumetric heat source and temperature dependent material properties. The thermo-fluid model will be solved by energy and flow equations and incorporates Marangoni effect whereas thermal model is purely based on energy equation. The thermo-fluid

model was firstly validated against the experimental results. In addition, the melt pools of thermal model with tested effective thermal conductivities were compared with the melt pool of thermal-fluid model and experimental results. The study of effective thermal conductivity can help us predict the EBAM process thermal characteristics with much less computational effort and reasonable accuracy.

2. Methodology

2.1. Overall Methods

In order to accurately capture fluid dynamics in the melt pool, Finite Volume Method (FVM) is used to simulate the heat transfer and solidification/melting process. There are some assumptions for the model to simplify the simulation process. The melt pool was assumed to be Newtonian incompressible liquid with laminar flow. The powder layer was considered as a continuum media with powder material properties. The powder bed shrinkage which occurs due to porous powder medium was neglected in the study. Convection heat transfer between Ti-6Al-4V domain and atmosphere was ignored as the powder melting occurs in vacuum environment. The melt pool surface was considered to be constantly flat while Marangoni phenomenon was still included in the model.

2.2. Thermal-fluid model and simulation

Governing equations:

In EBAM process, heat and mass transfer occurs by conduction and melt pool flow. Thermo-fluid model with heat transfer and fluid flow equations are developed to predict the temperature and melt pool flow. The governing differential equations that describe fluid flow with heat transfer include mass, momentum and energy conservation equations. The continuity equation in this model is presented in equation (1).

$$\frac{\partial \rho}{\partial t} + \frac{\partial(\rho u_i)}{\partial x_i} = 0 \quad (1)$$

Where ρ is density, t is time, x_i and u_i are the distance and velocity along the Cartesian directions, respectively.

In this study, the medium is assumed to be continuum and the influence of the loose powder on the fluid convection as well as the momentum is neglected. Equation (2) is the governing momentum equation applied in this model.

$$\frac{\partial(\rho u_j)}{\partial t} + \frac{\partial(\rho u_i u_j)}{\partial x_i} = \frac{\partial}{\partial x_i} \left(\mu \frac{\partial u_j}{\partial x_i} \right) + S_j \quad (2)$$

Where μ is the viscosity, S_j is the source term for the j th momentum equation.

The solidification and melting model is used to take into account the melting of powder above liquidus temperature and solidification below the solidus temperature. The liquid fraction is calculated using equation (3).

$$\beta = \frac{T - T_{solidus}}{T_{liquidus} - T_{solidus}} \quad (3)$$

In order to accurately capture the transient heat transportation phenomenon in the EBAM process, the heat source has been modeled as a moving Gaussian distribution heat source in

horizontal direction with a linear decaying in vertical direction[7]. This source term is applied to the energy equation as shown in equation (4).

$$\frac{\partial(\rho H)}{\partial t} + \frac{\partial(\rho u_i H)}{\partial x_i} = \frac{\partial}{\partial x_i} \left(k_{eq} \frac{\partial T}{\partial x_i} \right) + \dot{Q}(x, y, z) \quad (4)$$

Where,

$$\dot{Q}_{(x,y,z)} = \eta \times \frac{H_s \times I_z}{S} \quad (5)$$

with

$$I_z = \frac{1}{0.75} \left(-2.25 \left(\frac{z}{S} \right)^2 + 1.5 \left(\frac{z}{S} \right) + 0.75 \right),$$

$$H_s = \frac{2W}{\pi d^2} \exp \left\{ -\frac{2[(x-x_s)^2 + (y-y_s)^2]}{d^2} \right\}.$$

In which the parameters include electron beam absorption efficiency coefficient: η , power: W, optical penetration depth: S, laser spot size: d, xs and ys: heat source center position. H_s and I_z are horizontal Gaussian distribution heat source and heat source magnitude decaying function in vertical direction, respectively. A user defined subroutine was developed to incorporate the heat source domain and magnitude in the model.

Model configuration:

3D thermal and thermo-fluid models were developed using ANSYS Fluent software. Figure 1 shows the geometry and detailed view of a portion of the geometric model, which has a solid substrate dimension of $20 \times 3 \times 10$ mm (length, width, and height) as previously deposited material. The top layer of $70\mu\text{m}$ is defined over the solid substrate to represent the newly deposited powder particles. Fine mesh of element size $0.02 \text{ mm} \times 0.02 \text{ mm} \times 0.01 \text{ mm}$ was defined for the powder layer and relatively coarser mesh was applied to the region away from scanning area, as shown in Figure 1. All the elements in the model are hexahedron type. Conical volumetric heat source is applied and controlled by user defined function. Typical EBAM process parameter used for model simulation is shown in table 1. Temperature dependent material properties [7]: density, thermal conductivity and specific heat are used in the model to improve prediction accuracy. The 3D model geometry, size, material properties, mesh sizing was same for both thermal and thermo-fluid model. The thermo-fluid model predicted temperature and fluid flow by solving energy and flow equation. Marangoni effect was also incorporated whereas in thermal model, flow equation was deactivated and effective thermal conductivity was utilized.

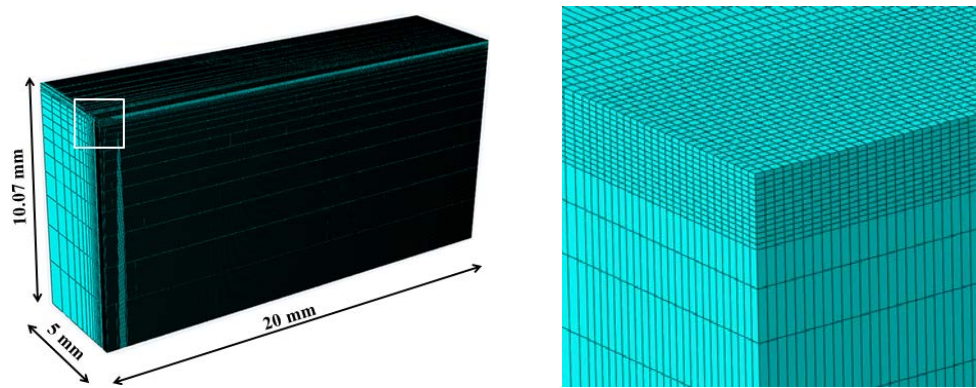


Figure 1: 3D numerical model for thermal and thermal-fluid simulation with detailed view.

Table 1: Parameters used in simulation

Parameters	Values
Solidus temperature, T_S (°C)	1605 [13]
Liquidus temperature, T_L (°C)	1655 [13]
Latent heat of fusion, L_f (kJ/Kg)	440 [13]
Beam diameter, Φ (mm)	0.55
Absorption efficiency, η	0.9 [14]
Scan speed, v (mm/sec)	632.6
Acceleration Voltage, U (KV)	60[15]
Powder layer thickness, t_{layer} (mm)	0.07
Emissivity, ε	0.7 [16]
Porosity, φ	0.5
Beam penetration depth, d_P (mm)	0.062 [6]
Preheat temperature, $T_{preheat}$ (°C)	730
Viscosity(kg/m-s)	0.049[17]
Surface tension gradient (N/m-K)	-0.00026 [8]
Stefan-Boltzmann constant (W/m ² K ⁴)	5.67×10^{-8}

2.3. Thermal modeling with effective thermal conductivity

It has been demonstrated that the melt pool of thermo-fluid model would become wider, longer but shallower due to Marangoni effect with a lower maximum temperature, when compared to thermal model if thermal conductivity is not adjusted [8]. The convection heat transfer will be ignored if the flow effect caused thermal conductivity change in melt pool is not considered. Therefore, effective thermal conductivity in the melt pool, which will integrate the convection heat transfer into thermal model, has been investigated in this study. Moreover, only one value of effective thermal conductivity will be considered above melting point for simplification purpose. Figure 2 shows how effective thermal conductivity is defined for material used in thermal model. In thermo-fluid model, liquid thermal conductivity was from literature [18] whereas the effective thermal conductivity is a single value which is same for all liquid and independent of temperature.

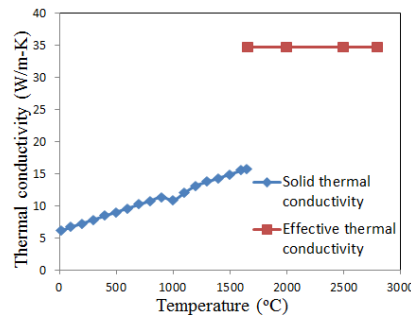


Figure 2: Example of effective thermal conductivity above melting point.

2.4. Comparison and determination of effective thermal conductivity

The determination of effective thermal conductivity value relies on iterative trial-and-error simulation process. The thermo-fluid simulation and experimental results are used as the

basis to formulate the effective thermal conductivity. At first, a sensible value is selected to carry out thermal simulation and result was compared with thermo-fluid simulation result. Modification to the effective thermal conductivity was made according to the compared result: the value of conductivity was increased if the maximum temperature in thermal simulation was higher than that of thermo-fluid simulation. Then an effective thermal conductivity corresponding to the validated thermo-fluid model was determined for thermal model.

2.5. Evaluation of property sensitivity and effect of process parameters

Variation in some of the material thermal properties may highly affect the thermo-fluid simulation result. To understand the role of different material properties in melt pool size and temperature distribution, sensitivity study of these properties on thermo-fluid simulation was conducted. Similarly, effects of process parameters were also studied. Different beam speed and beam diameters were used to carry out thermo-fluid simulations. Speed function (SF) is a system specific setting used in EBAM process. Different speeds corresponding to different SF indices at a certain build height have been determined [19]. Four speeds, 481 mm/s (SF20), 853 mm/s (SF36), 1193 mm/s (SF50) and 1595 mm/s (SF65), were incorporated in the model to carry out the thermal and thermal-fluid speed effect simulation. In addition, different beam diameters (0.55 / 0.65 / 0.75 mm) and different beam currents (4.8 / 7.7 mA) were used to study beam diameter and current effect. These specific parameters were selected so as to make comparison with experimental data [19].

3. Results and Discussion

3.1. Typical simulation results

Single track simulations have been performed for both thermal and thermo-fluid model. Typical temperature distributions are shown in figure 3. It is observed that the moving beam will continuously melt the powder region in the periphery of the beam center where the temperature is above melting point of Ti6Al4V. It can be seen that the thermo-fluid simulation results, both melt pool and temperature distribution are comparable to experimental results. The thermo-fluid simulation resulted in a melt pool length, width and depth of 3.04 mm, 1.04 mm and 0.112 mm, while experimental melt pool length and width are ~2.74 mm and ~0.72 mm [7]. The effective conductivity was used in thermal model for same set of process parameters. In this model, flow equation was turned off and no-slip condition was applied at the scanning surface. The effective thermal conductivity was adjusted to match the maximum temperature of the thermo-fluid model. Different effective conductivity values were tested: 30 W/m-K, 34.75 W/m-K, 35 W/m-K, and 40 W/m-K. It is observed that at effective conductivity of 34.75 W/m-K, the maximum temperature of 2754°C is obtained. The melt pool length and width obtained with this method is 2.34 mm and 0.88 mm. The melt pool characteristics of thermal and thermo-fluid model comparison with experiment result are presented in figure 4.

The melt pool length and width of thermo-fluid simulation is larger compared to that of thermal model. This may be due to the Marangoni effect in thermo-fluid model which results in the outward flow of the melt pool. Another reason for the shorter melt pool length could be due to faster cooling at the tail region as a result of high effective thermal conductivity. The resulted

melt liquid flow velocity field is shown in figure 5. An outward flow is observed due to negative temperature coefficient of surface tension. It can be seen that the velocity is lower at the center and increases at the edge of the melt pool. For a typical simulation using two Intel(R) Xeon(R) CPUs, thermo-fluid simulation took approximately 23 hours to complete while it took only about one hour for thermal simulation. The significant reduction of simulation time demonstrates the computational advantage of using thermal model.

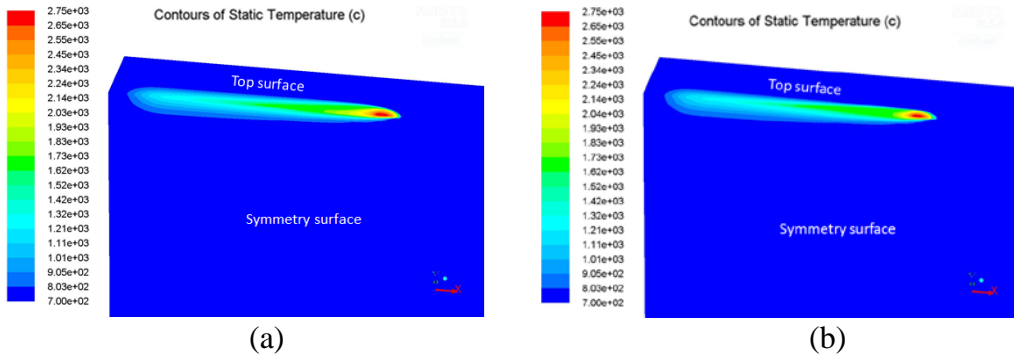


Figure 3: Temperature distribution in thermo-fluid simulation (a) and thermal simulation with effective thermal conductivity (b).

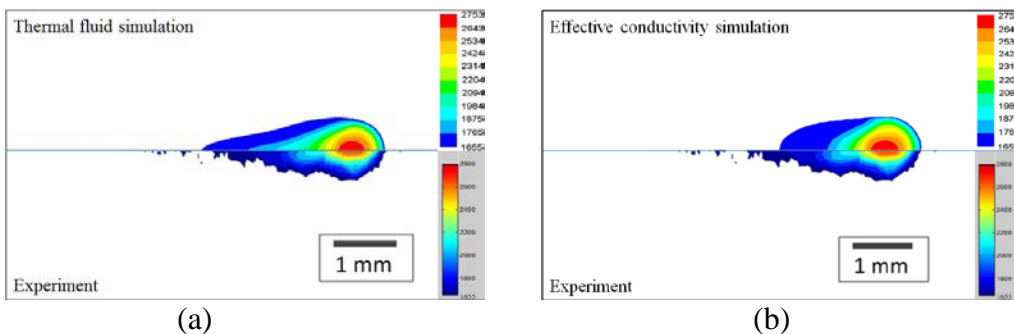


Figure 4: Melt pool characteristics comparison with experiment: thermo-fluid model(a) and thermal model(b).

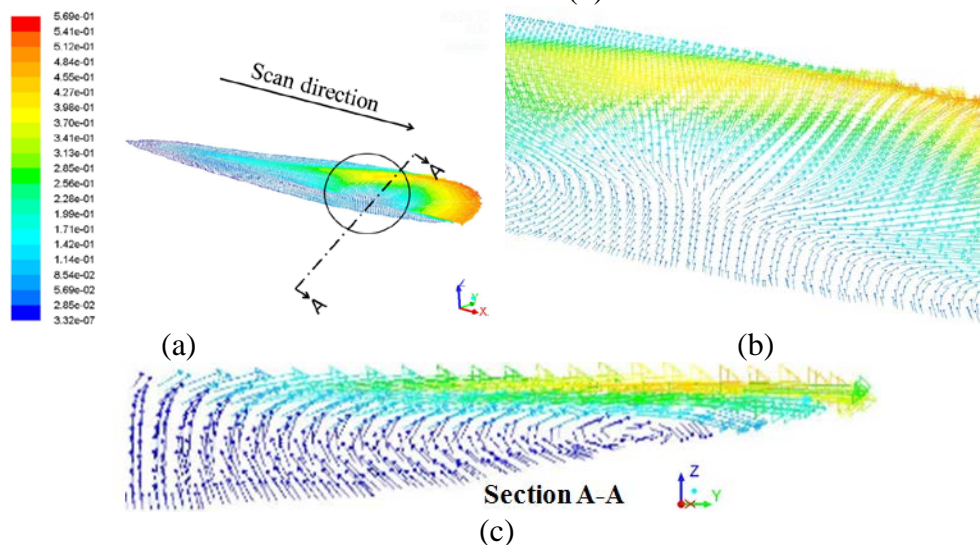


Figure 5: Velocity profile (m/s) at molten pool (a), detailed velocity profile at the beam center (b) and cross sectional view at beam center(c).

3.2. Sensitivity to material properties

Material property sensitivity study has been conducted to test individual factor effect. Flow properties such as viscosity and surface tension can define the hydrodynamics and transport phenomena of melt pool. These values are varied to check their influence on melt pool characteristics. Different literatures have reported different Ti6Al4V viscosity: 0.00236 Pa-s [8], 0.0049 Pa-s [20] and 0.049 Pa-s [17]. The sensitivity of thermo-fluid model with respect to these viscosity values are performed, simulations are carried out and resultant melt pool information are shown in figure 6. It is observed that the increase in length is significant with the increase of viscosity which may be due to increase in momentum of the molten pool. It can be said that thermo-fluid simulation is very sensitive to fluid viscosity.

Similarly, increasing the surface tension effect increases the outward flow or convection heat transfer thereby decreasing resultant maximum temperature of the system. Different surface tension coefficient can be found in different literatures: -3.6e-04 N/m-K [21] and -2.6e-04 N/m-K [8]. Besides, surface tension was increased and decreased ten times from -2.6e-04 N/m-K to amplify its effect on melt pool characteristics. When the surface tension coefficient was increased to -2.6e-03 N/m-K, the convection heat transfer became dominant and nearly round melt pool shape was obtained. The two surface tension values obtained in literature have close melt pool characteristics, while a significantly larger surface tension value may reduce the melt pool length but increase melt pool width such as -2.6e-3 N/m-K case.

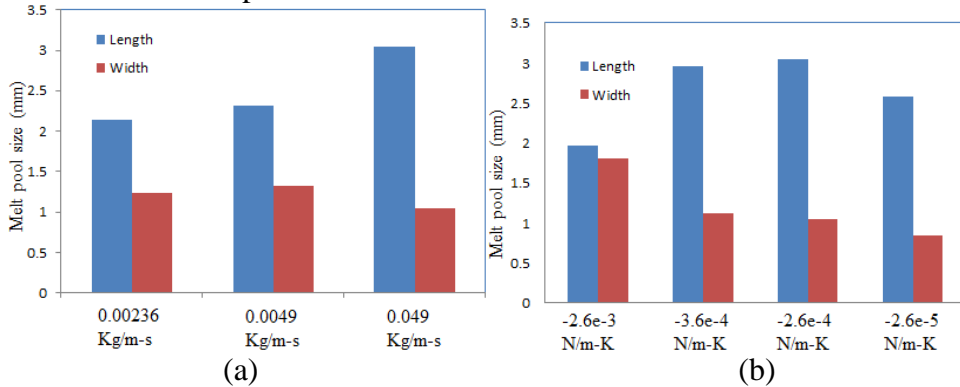


Figure 6: Effect of material properties: viscosity (a) and surface tension (b) on melt pool size.

3.3. Process parameter effects

Beam speed effect:

Both thermal and thermo-fluid simulations were carried out for four different SF cases and melt pool sizes have been compared with the experimental result, as shown in figure 7. It is observed that with increasing speed the temperature of the system decreased, and the melt pool size decreased accordingly. At SF20 (481 mm/s), the melt pool length in thermo-fluid model was very long. Here, the effect of Marangoni convection seems to be highly dominant: at low velocity, the energy density in the melt pool is higher which may have increased the temperature gradient and greatly induced the surface tension effect. The thermal model with effective thermal

conductivity has melt pool size close to the experimental results. The thermal model is case dependent: for some cases it under-predicts whereas for some other it over-predicts. The diameter decreased almost linearly with increasing velocity. The accuracy of the thermal model depends on the process parameter. The error percentage obtained for each speed with respect to experiment is plotted in figure 7. In regards of melt pool length, maximum error of 25% was observed for speed 1595 mm/s. However, for melt pool width, a maximum error of 7.3 % was recorded when beam speed was 1193 mm/s. Based on the beam speed effect study, we can say that use of effective thermal conductivity may be a reasonable approach.

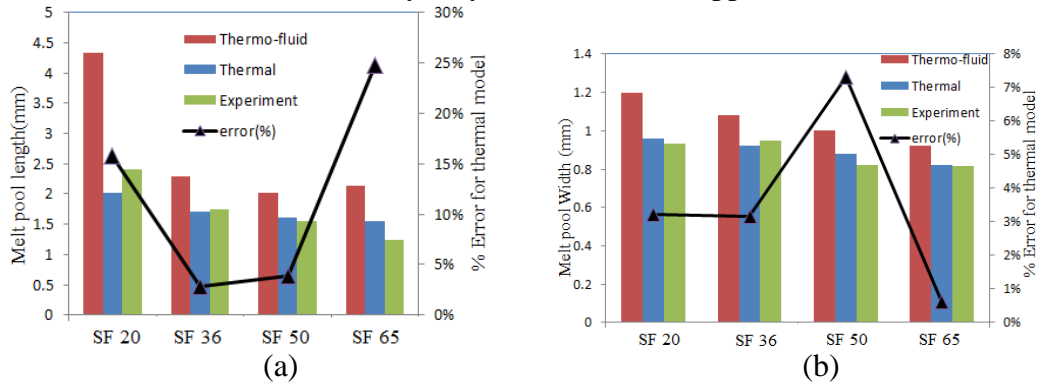


Figure 7: Melt pool length (a) and width (b) comparison between simulation and experiment for different beam speed.

Beam diameter effect:

The beam diameter effect is also studied with three beam diameters: 0.55 mm, 0.65 mm and 0.75 mm. The beam speed and beam current used for this study was 671 mm/s and 6.7 mA respectively. Thermo-fluid simulation always had higher length and width compared to thermal simulation as shown in figure 8. The decrease in length with increase in diameter of the beam may be because of decreased energy density in the radial direction. In addition, the increase in melt pool width is the result of energy being distributed over larger area with increasing diameter. Moreover, the rate of diffusion behind the scan path is higher, because of solidified metal, compared to other direction as there is powder material in both sides and ahead of the scan path. The thermal model highly under-predicts the melt pool length for beam diameter 0.55 mm whereas for 0.65 mm, the melt pool length is reasonable. The maximum error (35%) occurred in prediction of melt pool length for 0.55 mm beam diameter. Melt pool length had error below 23%. Moreover, thermal and thermo-fluid simulation was carried out for beam diameter 0.75mm. The result show similar trend: melt pool size is bigger in thermo-fluid model.

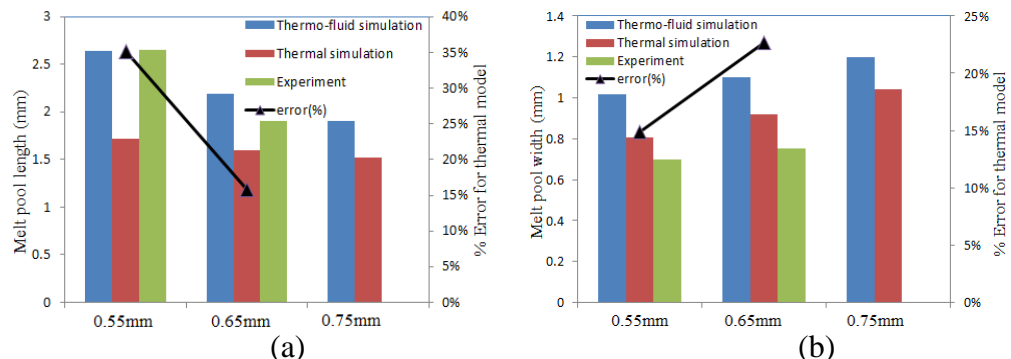


Figure 8: Melt pool length (a) and width (b) comparison between simulation and experiment for different beam diameters.

Beam current effect:

Two beam currents, 4.8 mA and 7.7 mA, were used to analyze the beam current effect on the melt pool. Beam diameter of 0.65 mm and beam speed of 505.5 mm/s were used. The simulated melt pool size has been compared with the experimental results in figure 9. Thermal simulation with effective conductivity is in more agreement with the experiment result compared to thermo-fluid simulation. For current 7.7 mA, the melt pool length predicted by thermo-fluid model is nearly double the experiment result. This may be the result of increase in power. As seen in SF 20 case, when the energy density increased, the surface tension effect became dominant and the outward flow increased. However, for low current, thermo-fluid simulation is in more agreement with the experiment results.

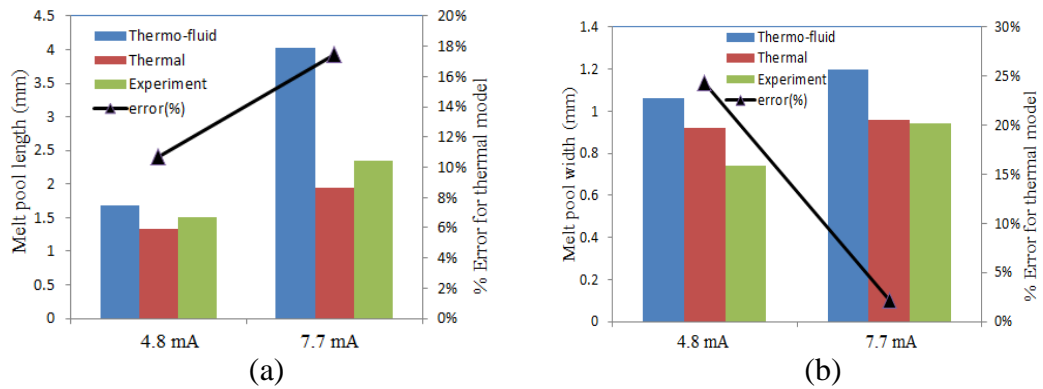


Figure 9: Melt pool length (a) and width (b) comparison between thermo-fluid simulation and experiment.

4. Conclusions

This study focuses on effective thermal conductivity which may be used to predict thermal characteristics of powder bed EBAM process. A 3D thermo-fluid model was developed to predict temperature and melt flow during EBAM process. The Marangoni effect has been included which may result in an outward flow of the melt pool. The thermo-fluid melt pool has a dimension of 3.04×1.04 mm (length \times width) which is in fair agreement with the experiment results of 2.74×0.72 mm. Then, the thermo-fluid model was used as the basis to formulate effective thermal conductivity for thermal model. Based on the study, an effective thermal conductivity of 34.75 W/m-K could result in similar thermal response as that of thermo-fluid model. However, melt pool sizes obtained from effective conductivity cases were smaller compared to experiments. The major findings can be summarized as:

(1) Specifically, the accuracy of applied effective thermal conductivity depends on process parameter. The average error of 12% was obtained for four speeds tested. The melt pool width has better prediction with experimental result with maximum error of 7.5%. The maximum error recorded was 25 % for melt pool length.

(2) The magnitude of length error (35%) was high for 0.55 mm beam diameter case. However, 0.65 mm beam diameter case was in reasonable agreement with experiment. A reverse trend in width prediction has been observed whereas 0.55 mm case has a better prediction result.

(3) The melt pool length prediction for two beam current cases resulted errors below 20%. The accuracy highly deviated for melt pool width: 24% error for 4.8 mA and 2% error for 7.7 mA.

The effective thermal conductivity may be a reasonable approach based on the limited sets of this study. However, predicted errors varied from ~2.5% to ~25% for length and ~2% to 35% for width, which may indicate the effective thermal conductivity can be adjusted based on process parameters. Thus, more tests are needed to study the appropriateness of melt pool characteristics predicted using this method. Future work will also include the study of energy density effect on thermal fluid model. For high energy density case, e.g., 483 mm/s speed case, the thermal fluid highly over-predicted the melt pool size compared to experiment.

Acknowledgement

This research is partially supported by CFD Research Corporation.

References

- [1] Körner, C., Attar, E., and Heinl, P., 2011, "Mesoscopic simulation of selective beam melting processes," *Journal of Materials Processing Technology*, 211(6), pp. 978-987.
- [2] Yuan, P., and Gu, D., 2015, "Molten pool behaviour and its physical mechanism during selective laser melting of TiC/AlSi10Mg nanocomposites: simulation and experiments," *Journal of Physics D: Applied Physics*, 48(3), p. 035303.
- [3] Cheng, B., and Chou, K., 2015, "Melt Pool Evolution Study in Selective Laser Melting," 26th Annual International Solid Freeform Fabrication Symposium - An Additive Manufacturing Conference, Austin, TX, USA, August 10-12, 2015, pp. 1182-1194.
- [4] Zeng, K., Pal, D., and Stucker, B., 2012, "A review of thermal analysis methods in Laser Sintering and Selective Laser Melting," 23rd Annual International Solid Freeform Fabrication Symposium - An Additive Manufacturing Conference, Austin, TX, USA, August 6-8, 2012.
- [5] Mahale, T. R., 2009, Electron beam melting of advanced materials and structures.
- [6] Zäh, M. F., and Lutzmann, S., 2010, "Modelling and simulation of electron beam melting," *Production Engineering*, 4(1), pp. 15-23.
- [7] Cheng, B., Price, S., Lydon, J., Cooper, K., and Chou, K., 2014, "On Process Temperature in Powder-Bed Electron Beam Additive Manufacturing: Model Development and Validation," *Journal of Manufacturing Science and Engineering*, 136(6), p. 061018.
- [8] Jamshidinia, M., Kong, F., and Kovacevic, R., 2013, "Numerical Modeling of Heat Distribution in the Electron Beam Melting® of Ti-6Al-4V," *Journal of Manufacturing Science and Engineering*, 135(6), p. 061010.
- [9] Mizikar, E. A., 1967, "Mathematical heat transfer model for solidification of continuously cast steel slabs," *AIME MET SOC TRANS*, NOV. 1967, 239, 11, P 1747- 1758.
- [10] Oksman, P., Yu, S., Kytönen, H., and Louhenkilpi, S., 2014, "The Effective Thermal Conductivity Method in Continuous Casting of Steel," *Acta Polytechnica Hungarica*, 11(9), pp. 6-22.
- [11] Taylor, G. A., Hughes, M., Strusevich, N., and Pericleous, K., 2002, "Finite volume methods applied to the computational modelling of welding phenomena," *Applied Mathematical Modelling*, 26(2), pp. 311-322.

- [12] De, A., and DebRoy, T., 2013, "Improving reliability of heat and fluid flow calculation during conduction mode laser spot welding by multivariable optimisation," *Science and Technology of Welding & Joining*.
- [13] Welsch, G., Boyer, R., and Collings, E., 1993, *Materials properties handbook: titanium alloys*, ASM international.
- [14] Rouquette, S., Guo, J., and Le Masson, P., 2007, "Estimation of the parameters of a Gaussian heat source by the Levenberg–Marquardt method: application to the electron beam welding," *International Journal of Thermal Sciences*, 46(2), pp. 128-138.
- [15] Gaytan, S., Murr, L., Medina, F., Martinez, E., Lopez, M., and Wicker, R., 2009, "Advanced metal powder based manufacturing of complex components by electron beam melting," *Materials Technology*, 24(3), pp. 180-190.
- [16] Yang, J., Sun, S., Brandt, M., and Yan, W., 2010, "Experimental investigation and 3D finite element prediction of the heat affected zone during laser assisted machining of Ti6Al4V alloy," *Journal of Materials Processing Technology*, 210(15), pp. 2215-2222.
- [17] Elmer, J., Palmer, T., Babu, S., Zhang, W., and DebRoy, T., 2004, "Phase transformation dynamics during welding of Ti–6Al–4V," *Journal of applied physics*, 95(12), pp. 8327-8339.
- [18] Mills, K. C., 2002, *Recommended values of thermophysical properties for selected commercial alloys*, Woodhead Publishing.
- [19] Price, S., Cheng, B., Lydon, J., Cooper, K., and Chou, K., 2014, "On Process Temperature in Powder-Bed Electron Beam Additive Manufacturing: Process Parameter Effects," *Journal of Manufacturing Science and Engineering*, 136(6), p. 061019.
- [20] Yang, M., Yang, Z., and Qi, B., 2015, "Effect of fluid in molten pool on the welds with Ti-6Al-4V during pulsed arc welding," *The International Journal of Advanced Manufacturing Technology*, 81(5-8), pp. 1007-1016.
- [21] Egry, I., Holland-Moritz, D., Novakovic, R., Ricci, E., Wunderlich, R., and Sobczak, N., 2010, "Thermophysical properties of liquid AlTi-based alloys," *International Journal of Thermophysics*, 31(4-5), pp. 949-965.